Viscoelastic Recovery Behavior Following Atomic Force Microscope Nanoindentation of Semicrystalline Poly(ethylene)

Davide Tranchida, Zebene Kiflie, and Stefano Piccarolo*

Dipartimento di Ingegneria Chimica dei Processi e dei Materiali, Università di Palermo, Viale delle Scienze, 90128 Palermo, Italy & INSTM Udr Palermo

Received March 21, 2007; Revised Manuscript Received July 12, 2007

ABSTRACT: The residual imprint left behind by the AFM nanoindentation of polymers has been seldom studied in the past. In this work, the evolution of indentations at room temperature performed on a semicrystalline poly(ethylene) in a broad range of experimental conditions is presented. The study shows that the recovery after 24 h is substantial, although not complete. Moreover, the dynamics of the recovery process is not seen to depend on the magnitude of the applied load for the nanoindentation, but instead on the rate of the indentation used. This points out that viscoelastic processes are minimized when performing fast nanoindentations, while at low loading rates there seems to be a residual viscoelastic energy stored in the system. Although, the recovery process involves complex displacements and bending of crystalline lamellae, which is difficult to model theoretically, the present work attempts to quantify the magnitudes as well as the directions of such displacements for indentations involving from two to seven lamellae.

Introduction

The AFM nanoindentation test is increasingly becoming a standard and useful tool for probing mechanical properties of thin films and complex samples characterized by the distribution of structures.

As a matter of fact, the possibility to test mechanical properties on nanometer scale allows one to conjugate fundamental knowledge on morphology, coming from unprecedented high-resolution images of soft matter, with the information on mechanical performance. For example, the reliability of such measurements has been proven in the past on very different polymeric systems, such as poly(urethane)-,[1] poly(styrene)-,[1] poly(vinyl chloride)-,[1] poly(ethylene)-,[2] poly(propylene)-,[2] poly(carbonate)-,[2] poly(isoprene)-,[1] and poly(propylene glycol)-based rubbers.[2,3] It was found that Young's moduli for homogeneous samples matched those obtained from nanoindentations, made under specific properly identified experimental conditions in such a way that the mechanical behavior becomes essentially elastic,[2] i.e., with negligible contribution from more complex mechanical phenomena like viscoelastic or irreversible ones. These experimental conditions mainly stem on the use of high loading rates, because the residual indentation imprint left behind by the indenter is much smaller than the penetration depth under full load (less than one tenth), thus allowing the use of elastic contact models such as those of Hertz,[4] Sneddon,[5] and Segedin.[6]

In fact, although some limitations have been reported,[7] once the contact geometry is known,[8] the application of these approaches has led to the analysis of several soft materials, polymers as well as biologic systems.[9−12]

Moreover, few works have attempted at exploring the effect of viscoelasticity on nanoindentations. Tsukruk et al.[13] tested several polymers, showing that the effect of indenter rate on Young's moduli could satisfactorily be fitted with a WLF (William, Landel, and Ferry) approach to link temperature and loading rate, although the experimental evidence was limited to room temperature. These experiments were also extended to temperatures up to 51 °C on amorphous poly(*n*-butyl methacrylate)[14] observing that the mechanical behavior is different depending on temperature and loading rates, and this could apparently be related to the viscoelastic response of the material. However, it is worth to mention the residual imprint is not anymore small compared to penetration depth at full load pointing out the onset of dissipative processes.[2]

As shown in a previous study,[2] made on a variety of amorphous and semicrystalline polymers, slow indentations resulted in residual depths as much as half of the penetration depth under full load. Under such conditions, therefore, it becomes hard to justify the use of simple elastic models since plasticity, viscoplasticity, and long-term viscoelastic behavior are present when indenting polymeric materials.

In spite of all these contributions, the exact nature and evolution of the residual imprint is however not yet clear. Usually, for polymer samples, indentation depth keeps on decreasing, possibly vanishing at very long times depending on sample characteristics suggesting that the residual indentation depth imaged by the AFM after indentation is not only a plastic feature but has to be related to the viscoelastic behavior of the material as well. In order to overcome the limitation arising from long-term recovery behavior, two different poly(propylene glycol)-based rubbers, already shown to behave as ideal rubbery networks in proximity of room temperature, were studied in a parallel work[3] to explore the study of viscoelasticity during nanoindentations. The absence of any residual imprints, at least on the scale that the AFM can image, strongly pointed in favor of the occurrence of purely elastic contact or, better, toward the absence of any long-term viscoelastic behavior. In this case, the temperature dependence of the Young's modulus during the glass transition was studied and successfully compared to macroscopic mechanical tests.[3] Activation energy for the collective and elementary motions, in the glassy and rubbery regions respectively, were also in agreement with typical expected values for rubbers.[3]

The study of nonideal systems, however, is still a challenging issue because of the complexity to describe, from a mathematical standpoint, the occurrence of several and so different mechanical processes in the framework of contact mechanics.

* Corresponding author. E-mail: piccarolo@unipa.it.

10.1021/ma070682b CCC: $37.00
Published on Web 08/29/2007

To our knowledge, only a few papers[15−17] investigated the recovery behavior of indents, in the framework of a study about dewetting and the ability to heal dry patches. In particular, nanoindentations were performed on thin films (below 100 nm) of poly(styrene)'s with molecular weights ranging from 13700 to 29300 and then annealed above the glass-to-rubber transition. Indents on disentangled PS were found to level quickly, resulting in a flat polymer surface after time spans ranging from 10 min to few hours depending on the molecular weight. In this case, the healing was successfully related to the local mean curvature of the indent and thus interpreted as a diffusion-driven phenomenon. As far as the behavior of high molecular weight samples, more relevant to the results to be discussed in this work, the dynamics of the recovery was found to be different, leading to a different dependence on annealing time with respect to the low molecular weight samples. The relaxation of the residual stress, thus a viscoelastic effect, was identified as the main cause of the difference in the recovery dynamics.

A semicrystalline HDPE, characterized by the onset of relatively easy-to-image regular stacks of lamellae, was analyzed in this work. Because of its fast crystallization kinetics HDPE crystallizes with a morphology of poorly interconnected well developed lamellae whose deformation, under the AFM tip, can easily be followed since the bent has a geometric resemblance with the AFM tip shape.

The aim of this work is the study of the imprint evolution with time, in order to highlight the inherent phenomena and the complexity of the required mechanical analysis. The possibility to image the single deformed lamellae, moreover, allowed us to visualize the positions of the lamellae during the recovery process, showing for the first time the complex effect of morphology on the recovery extent and dynamics.

Experimental Section

The material used was a research grade HDPE, kindly supplied by SABIC, with $M_n = 11000$ g/mol, $M_w = 280000$ g/mol, and $M_z = 1500000$ g/mol. Samples have been prepared by slow cooling from the melt followed by isothermal annealing at 100 °C in a hot-stage controlled by a Mettler-Toledo FP82HT with FP90 central processor and fluxed with nitrogen. The annealing process made it possible to obtain a stable, fully developed semicrystalline structure characterized by stacks of crystalline lamellae embedded in the amorphous matrix.

Tapping-mode AFM images were obtained using a NanoScope IIIA MultiMode AFM (Digital Instruments). All the experiments were run under an air atmosphere at constant ambient temperature of 25 °C within 24 h from the sample preparation. Si cantilever tips (TESP) having a resonance frequency of approximately 300 kHz and a spring constant of about 40 N/m were used. Furthermore, the cantilever elastic constant was in any case estimated according to Green et al.[18] so as to correctly evaluate the applied load used for nanoindentations. Deflection sensitivity of the optical lever system was measured by indenting a hard substrate, namely a silicon wafer. Loads for nanoindentations ranged from ca. 0.3 μN up to 3 μN, while indenter rate ranged from 90 up to 10000 nm/s

The scanning rate used was relatively high (approximately 5 Hz) for collecting the very first images after the nanoindentations, in order to capture the short-term recovery behavior. Afterward, scan rate of about 2 Hz was used, as a compromise between the proper AFM setup and sufficient time resolution of the measurements.

The typical value for the amplitude was 2.0−2.5 V, and the set point amplitude ratio r_{sp} (A_{sp}/A_o, where A_{sp} is the set-point amplitude and A_o is the amplitude of the free oscillation) was adjusted in the range of 0.6 to 0.8. The amplitude and set-point ratios were carefully chosen, specially at high scan rates, such that the surface was tracked while maintaining the necessary quality and contrast in the images[19] thus ruling out the onset of instabilities which could determine the presence of artifacts. The AFM images were obtained immediately after the nanoindentations, in order to capture the dynamics of the recovery with the same tip used for indentations. The minimum time for collecting an image was in the order of a few minutes for a good resolution to be obtained. During this time lapse, the sample recovers at least half of the deformation under full load so that the imprint becomes blunter than the tip. This means that convolution effects of tip shape during imaging can be neglected.

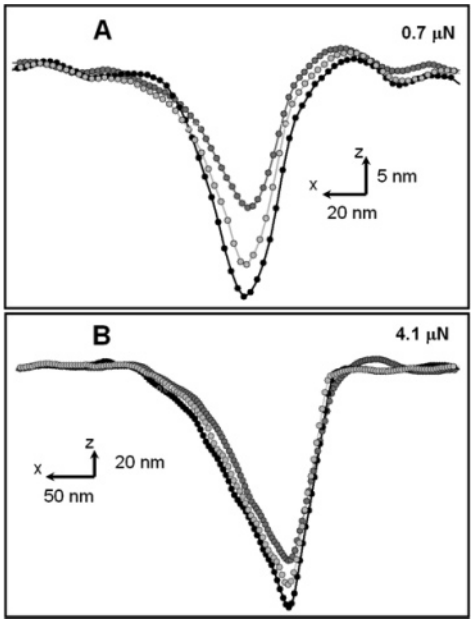

Figure 1. Evolution of the indent profile, few minutes after the indentation (black series), 400 min (light gray), and 24 h (dark gray), with an applied load of 0.7 (A) and 4.1 (B) μN.

Phase images were also collected, which provide additional information about the material properties being imaged and better visualization of morphological details. Under the imaging conditions used for these studies, hard materials appear light, while sticky and soft materials appear dark, giving a contrast between the crystalline and the amorphous material.

All images were processed using procedures for plane-fit in Nanoscope software version 5.30 (Digital Instruments) without any filtering. Dimensions of the indents and position of the lamellae were carefully measured on the profiles obtained by sections of the images with SPIP (Image Metrology) software.

Results and Discussion

Parts A and B of Figure 1 show some profiles obtained under extreme conditions, i.e., with nanoindentations performed at low and high peak loads, 0.7 and 4.1 μN respectively, and at low piezo rate, 90 nm/s. Here, it can be noted that, apart from the evident long-term viscoelastic recovery, the imprints show relatively sharp profiles. The convolution of tip shape on these profiles might thus misrepresent the measurements of residual depth, in particular shallower imprints would be imaged because of convolution effects. However, one can assume that the imprint shape follows the tip shape when the maximum load, i.e., penetration, is reached during nanoindentation. Afterward, during the unloading, the sample elastically recovers.[2]

The indent initially shows a triangular shape, while the vertexes of the triangle become round and continue the recovery until the indent takes a circular shape.[15−17] This is followed by a subsequent lateral expansion of the circle.[15−17] At the same time, indentation depth decreases and thus the motion of any point at the surface of the indent is the result of two components, i.e., in-plane and vertical.[15−17] However it is commonly assumed

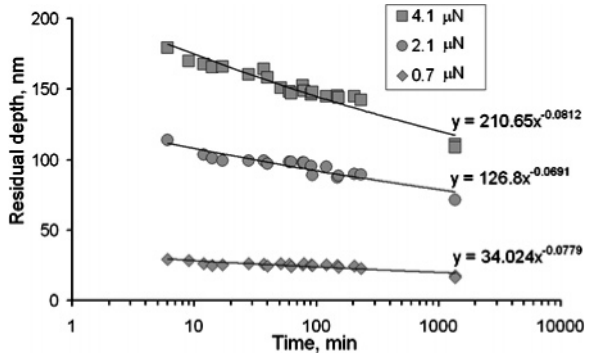

Figure 2. Dynamics of the recovery process, for nanoindentations performed at three applied loads, shows that residual depth is roughly half after 1000 min. The power law fitting exponent is similar irrespective of applied load.

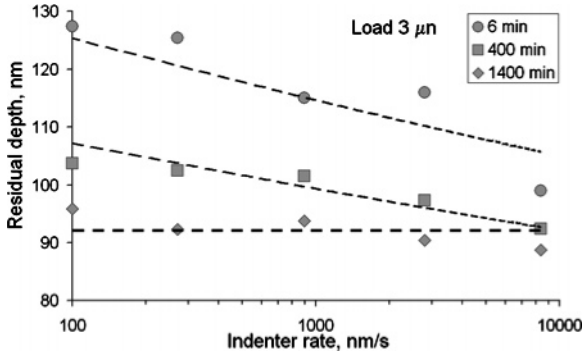

Figure 3. Recovery dynamics of imprints obtained from nanoindentations performed at different loading rates. Fast indentations imply low residual depth and low recovery, thus pointing out the elasticity of the contact. On the other side, slow nanoindentations result in larger indentation depths which recover quickly, pointing to the viscoelastic effects during both the nanoindentation and the recovery processes. Lines are a guide to the eye only.

that the in-plane deformation is only slightly recovered, while more significant is the recovery in the vertical direction.[20] The motion of the imprint apex is thus along the vertical direction. For this reason, most of the results presented in this work deal with the "residual depth" as measured by images of the imprints, in order to describe the viscoelastic recovery by means of a sensitive parameter and to simplify the analysis of the healing phenomenon.

The elastic recovery taking place during the unloading part of the AFM nanoindentation is substantial. For example, it was shown that for amorphous, semicrystalline and mesomorphic polymers the residual depth amounts to only one tenth of the penetration under full load when high loading rates are used.[2] Low loading rates, on the other hand, show a more limited elastic recovery, e.g., residual depth being as deep as half of the maximum depth under maximum load.[2] Although not shown here, the same trend has also been found on the material object of the present work. However, Figure 2 shows that the long-term viscoelastic recovery following slow indentations (indenter rate of 90 nm/s) is large at long times; e.g., the residual depth is found to be halved after 24 h, which means that the residual depth is approximately 25% of depth under a full load. It is worth to mention that the power law fitting of the plots in Figure 2 results in similar exponents, in the range of -0.07 to -0.08, and therefore the time dependence of the relaxation process does not depend on the initial depth, or equivalently on the applied load. It is imperative here to indicate that these results differ from those of Karapanagiotis et al.,[15−17] who reported, based on tests made on PS samples above the glass-to-rubber transition, that the recovery of the indentation depth followed an exponent close to -1.21 for low molecular weight disentangled PS and -0.3 for a high molecular weight grade. The considerable difference between the latter and our findings can be a result of the different loading rates used, see the discussion of Figure 3, as well as the difference in connectivity due to the presence of crystalline domains, i.e., lamellae, which act as physical cross-links.

One may thus wonder what the nature of the residual imprints is and which phenomena are involved therein. Figure 3 shows three plots of residual depth vs indenter rate, measured at three different times for the same applied load. It is clear that the use of high indenter rate results in smaller residual depth, which is slightly recovered with time. This implies that viscoelastic behavior is highly minimized under such conditions and the imprint is mostly the result of irreversible phenomena. On the other side, slow indentations give rise to the opposite behavior, i.e., a larger residual depth, which is recovered at a faster rate. In this case, it may be assumed that the elastic energy stored during the loading part is not released completely during the unloading part thus giving rise to the long-term viscoelastic recovery.

It is interesting to note that, although the same applied load gives different penetration depth under full load, as well as residual depth immediately after the nanoindentation depending on the time scale of the experiment, the residual depth tends to level off toward the same value after sufficient time, e.g., ca. 24 h in Figure 3. This could be interpreted as a plateauing effect due to contributions of plastic deformations, notwithstanding the indenter rate. This conjecture is reasonable, but other remarks need to be pointed out. At low loading rates, since the yield stress may be assumed to decrease, and the penetration depth under load is larger,[2] deformations would also be larger. This means that at low indenter rate the volume involved by plastic deformation is presumably bigger. Therefore, the leveling off of the residual depth (to approximately 90 nm in Figure 3) at long times is somewhat surprising and should rather be considered as a smearing, due to data dispersion, of the slight dependence of the onset of plasticity, i.e., yield stress, on deformation rate, i.e., on indenter rates.

The overall nanoindentation contact area is proportional to the square of the residual indentation depth, and therefore, the results in Figures 2 and 3 can be translated into nanohardness measurements. Indeed, hardness is defined as the ratio of applied load and a characteristic area measured from the residual imprint.[21] Depending on the choice for this area, two hardness definitions are usually calculated. The Meyer hardness makes use of the projection of the residual imprint, i.e., how it is visualized from an optical microscope image.[20] This represents a measure of the average contact pressure and, although preferred by physicists, its meaning is still under debate.[22] However, the measurement of Meyer hardness from a nanoindentation is difficult, since the edges of the imprint might be difficult to evaluate correctly. For example, the roundness of the edge imprint on such tiny scale can be confused with the intrinsic roughness of the sample, as can be perceived from Figure 1. Moreover, the rim around the indent relaxes quickly and the indent shape itself changes as discussed above, so that this measurement is somewhat troublesome. On the other side, the classical definition of hardness, like the Vickers hardness, stems on the overall contact area measured from the imprint and has been related to several materials' properties. Flores et al. highlighted the difference of polymers' microhardness with respect to other materials, so that the classical proportionality between hardness and yield stress has been questioned.[23] The

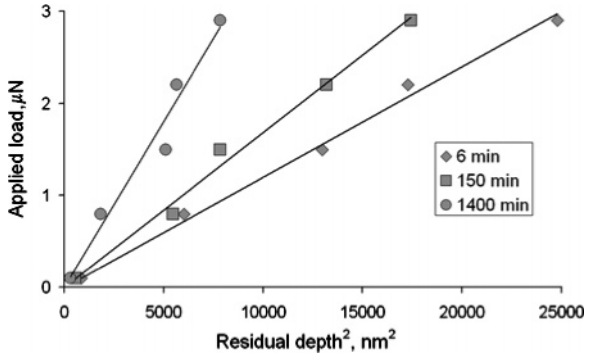

Figure 4. Slope of this plot is proportional to hardness, showing that this latter quantity apparently changes, depending on time.

Johnson model[24] allows the ratio of microhardness and yield stress to be related to a single nondimensional variable where the ratio of yield stress and the Young's modulus are present, revealing the influence of elastic strains. Following the Struik's model,[25] that relates the yield stress to the elastic modulus, Flores et al.[23] were thus able to evaluate the Young's modulus from microhardness experiments.

The plots of applied load vs indentation depth squared in Figure 4 should be linear in order to obtain a nanohardness value independent of applied load. The slope is in this case related to the hardness and a geometrical parameter. As it can clearly be seen, the plots are indeed linear, while the viscoelastic recovery causes the slope to increase and the apparent hardness also. It is worth to mention that the recovery in the vertical direction is larger than in the in-plane directions, as shown in Figure 1, and thus the proportionality factor (the tangent of the semi apex angle), relating the contact area and the indentation depth squared, increases. This means that the change in measured apparent hardness is smaller than perceived from the change in the slopes reported in Figure 4; however, Figure 1 clearly shows that contact areas do decrease with increasing time.

It was mentioned before that Flores et al. took into account the elasticity of the contact in order to properly predict the residual depth measured immediately after the nanoindentation through Johnson's and Struik's models, i.e., before any viscoelastic recovery takes place. The change in residual depth cannot however be linked anyhow to any change of elastic modulus with time, i.e., to viscoelasticity, through these models. This sets a serious limit to the hardness measurement from nanoindentation since (i) the values change and (ii) measuring immediately after the indentation, as commonly done, causes one to include viscoelastic effects which are not properly decoupled from plastic ones.

Images of six residual imprints, collected at different times and referred to different loads, are reported in Figure 5. Phase images usually allow one to achieve exceptional morphological details about semicrystalline polymers, due to the different interactions of the crystalline lamellae and the amorphous interlayers with the scanning tip. The background of Figure 5 has been intentionally saturated in order to better view the morphology within the imprint.

This effect could thus be attributed to a moderate interaction between the tip and the sample on the steep right side of the imprint with respect to the other indent side. It is worth to mention that Figure 5 depicts residual depth left by indentations performed at low indenter rate, 90 nm/s, as it was shown above that this experimental condition enhances the long-term recovery.

The in-plane dimensions of the imprints clearly decrease from Figure 5A to Figure 5C. The recovery process, described above only by the evolution of maximum residual depth measured on topography images, appears to be complex with a clear contribution of what we schematically identify with crystalline lamellae using them as tracers to follow vertical and in plane recovery of the deformation imparted during the nanoindentation.

In the case of the larger imprints in Figure 5A, upper left corner, the lamellae far from the point of maximum depth, and thus less deformed, completely heal the original deformation, Figure 5C. On the other hand, the lamellae subjected to the larger strains not only partially recover the vertical deflection, but also bend to high angles. The smallest imprint in Figure 5A, right top corner, consists of only two lamellae. One lamella completely heals in Figure 5C, while the other one shows some residual deformation although it is not bent. The systematic observation of the same features at very different times, with identical characteristics but for their position with time, is a further proof that they are not artifacts arising from poor instrumental settings, whose optimization precluded their onset.

Further insight on the displacements of the single lamellae can be achieved by simultaneous sections of the topography and the phase images, in order to observe, the two superimposed profiles. Lamellae in the phase image profile corresponds to spikes, see the gray profile in Figure 6, which then unambiguously identifies the position of the lamella on the topography, i.e., on the black profile in Figure 6.

The evolution of the recovery process for the diverse lamellae at two stages, i.e., after 400 and 1400 min, is shown in Figure 7. In this case, lamellae are subsequently numbered starting from those at larger indentation depth, i.e., lamellae with lower indices in Figure 7 are those most deformed. The vertical recovery at intermediate time, 400 min, with respect to the images collected immediately after the nanoindentations is more or less constant for the various lamellae, thus irrespective of the amount of starting deformation. However, for longer times, the two lamellae close to the point of maximum residual depth, i.e., the most deformed ones, recover less compared to the adjacent ones, probably due to the effect of dissipative processes taking place during the nanoindentation at the apex where stress concentration is larger. At the same time, the lamellae far away from the apex of the imprint slightly recover in absolute terms, since the starting deformation was not significant.

The recovery in the in-plane direction shows however a different trend. It can be seen in Figure 7 that, first of all, lateral displacements of the lamellae are noticeably smaller than vertical ones. Moreover, the limited recovery achieved at relatively short time, 400 min, is basically not improved at larger times, 1400 min, and remains constant. This means that the time scale of in-plane recovery is much shorter than the vertical one, although the magnitude of the recovery itself is more limited.

Figure 7 shows the recovery observed for the single lamellae at medium and long times. A more complete characterization of lamellae recovery rate is given in Figure 8. In this case, the vertical and lateral positions of the lamellae have been previously plotted against time and the resulting plots have been fitted with a power law relation, i.e.

$$x_{\text{lamella}} = k_x t^{n_x} \tag{1}$$

$$z_{\text{lamella}} = k_z t^{n_z} \tag{2}$$

The exponents, n_x and n_z, of these plots are reported in Figure 8, and we consider to be representative of the rate at which the recovery process for the single lamellae takes place. Vertical recovery in Figure 8 is a relatively fast process for all the

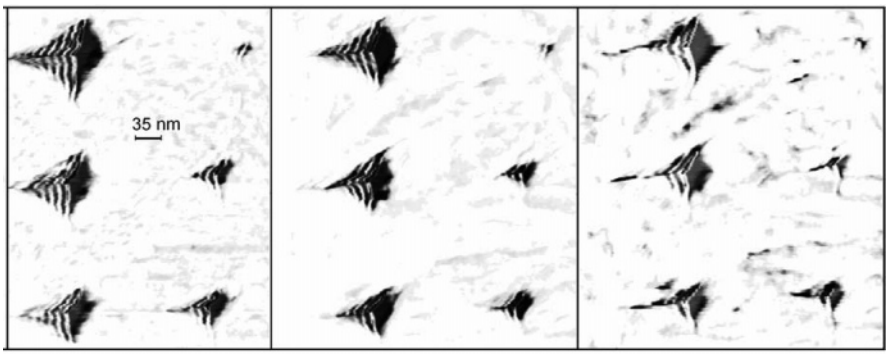

Figure 5. AFM phase images of the residual imprints clearly show the complex morphology evolution for nanoindentations performed at 0.7, 1.4, 2.1, 2.8, 3.5, 4.1 μN from top right clockwise respectively after 6 (A), 400 (B), and 1400 (C) min.

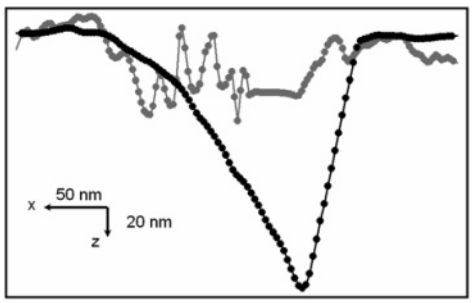

Figure 6. Simultaneous height (black) and phase (gray) profiles of a nanoindentation residual imprint. Lamellae appear as spikes in the phase profile.

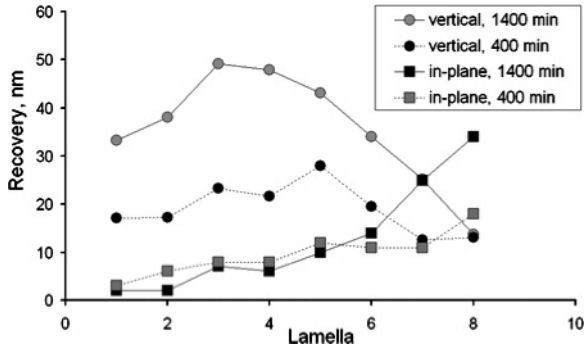

Figure 7. In-plane and vertical recoveries, with respect to initial positions, of each lamella after intermediate and long times. Low indices correspond to the most deformed lamellae, i.e., close to the apex of the AFM tip.

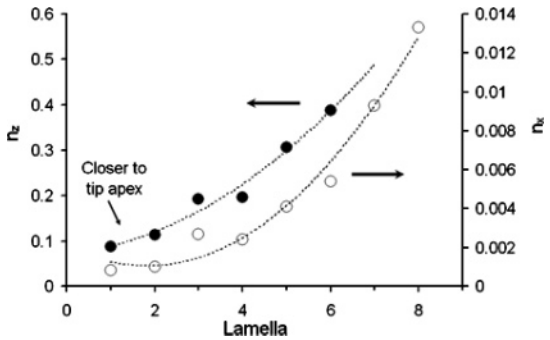

Figure 8. Rate parameters of the recovery processes show that the vertical one is much faster than the in-plane. Moreover, less deformed lamellae correctly show a faster recovery due to the negligible irreversible deformations.

lamellae, especially compared to the lateral recovery which is roughly four times smaller. Moreover, a clear trend is visible in Figure 8, such that the recovery of the most deformed lamellae is sensibly slower, up to a factor 4, than the less deformed ones. In this latter case, the smaller deformation imposed during the nanoindentation to the lamellae far from the AFM tip apex imply that these have undergone less plastic deformation and therefore the recovery dynamics is faster.

Conclusions

Knowledge of viscoelastic behavior of polymers on nanometer scale is of fundamental importance in a number of different fields, ranging from thin films to organic semiconductors.

The characterization of the elastic behavior through AFM nanoindentations has been subject of investigation by the present authors.[2] Conditions meeting the requirement of substantially elastic behavior have been identified. However, only few contributions can be found on the viscoelastic characterization due to the complex stress field arising in indentations. The most limiting difficulty encountered when analyzing the viscoelastic behavior during AFM nanoindentations is represented by the onset of plastic and long-term viscoelastic phenomena, i.e., mechanisms that cannot be separately identified either qualitatively or quantitatively from the force curve collected during a nanoindentation. Indeed, in several cases, the imprint left behind by the indenter recovers with time, up to total recovery, indicating the important role played by the viscoelastic polymer behavior.

A few contributions on the recovery of the indentation imprint of amorphous polymers, having a simple nanoscale homogeneous morphology can be found. However, to the best of our knowledge, similar studies on the viscoelastic recovery of the imprint after indentation for more complex semicrystalline polymers are missing.

For semicrystalline polymers, the dynamics of the recovery process, both in the in-plane and vertical directions, is substantially slower than for amorphous polymers even for high molecular weight poly(styrene), demonstrating the strong influence of connectivity due to the presence of crystalline lamellae which act as physical cross-links.

Modeling the trend of residual indentation depth vs time with a power law relation shows the exponent not to be dependent on the load, and therefore on the initial apparent residual depth, somewhat excluding the onset of nonlinear viscoelastic phenomena.

It is worth to mention that the present work on the recovery behavior is also useful in the framework of microhardness studies. Microhardness is indeed a parent technique of AFM nanoindentations and one of the simplest methods used to measure mechanical properties of materials on a local scale. The measurement is usually carried out following a specific protocol, as in ref 26, and the imprint left behind by the indenter, measured by optical microscopy, is taken as a measure of

plasticity, related to the yield stress, and, in the case of semicrystalline polymers, quantitatively related to crystallinity and crystal size. However, a significant recovery of the residual indent implies that, in the case of nanoindentations, i.e., using sharp indenters and fast indentations without holding, a microhardness like approach cannot be easily related to plastic properties only and the evaluation of viscoelastic contributions is fundamental.

Finally, the possibility to follow the recovery behavior of individual deformed lamellae has been made possible by the imaging capabilities of AFM. Imaging lamellae bent by nanoindentation is experimentally difficult to achieve. No such image, at least to our knowledge, has been shown so far. The present work has clearly shown that the vertical recovery of the single lamellae is greater but slower than the in-plane recovery. The latter can be considered as complete after ca. 400 min, while the former still takes place even after 1400 min. The dynamics of the recovery process of individual lamellae shows that the time constant for the vertical recovery is up to 4 times smaller than for the in-plane recovery.

References and Notes

(1) Chizhik, S. A.; Huang, Z.; Gorbunov, V. V.; Myshkin, N. K.; Tsukruk, V. V. *Langmuir* **1998**, *14*, 2606.
(2) Tranchida, D.; Piccarolo, S.; Soliman, M. *Macromolecules* **2006**, *39*, 4547.
(3) Tranchida, D.; Kiflie, Z.; Piccarolo, S. *Nanotechnology*, submitted.
(4) Landau, L. D.; Lifshitz, E. M. *Theory of Elasticity*; Pergamon Press: Oxford, U.K., 1986.
(5) Sneddon, I. N. *Int. J. Eng. Sci.* **1965**, *3*, 47.
(6) Segedin, C. M. *Mathematika* **1957**, *4*, 156.
(7) Tranchida, D.; Piccarolo, S. *Macromol. Rapid Commun.* **2005**, *26*, 1800.
(8) Tranchida, D.; Piccarolo, S. *Meas. Sci. Technol.* **2006**, *17*, 2630.
(9) Tranchida, D.; Piccarolo, S. *Macromol. Rapid Commun.* **2006**, *27*, 1584.
(10) Tranchida, D.; Piccarolo, S. *Polymer* **2005**, *46*, 4032.
(11) Fang, T.-H.; Chang, W.-J.; Tsai, S.-L. *Microel. J.* **2005**, *36*, 55.
(12) Ebenstein, D. M.; Pruitt, L. A. *NanoToday* **2006**, *1*, 26.
(13) Tsukruk, V. V.; Gorbunov, V. V.; Huang, Z.; Chizhik, S. A. *Polym. Int.* **2000**, *49*, 441.
(14) Cappella, B.; Kaliappan, S. K.; Sturm, H. *Macromolecules* **2005**, *38*, 1874.
(15) Karapanagiotis, I.; Evans, D. F.; Gerberich, W. W. *Polymer* **2002**, *43*, 1343.
(16) Karapanagiotis, I.; Evans, D. F.; Gerberich, W. W. *Macromolecules* **2001**, *34*, 3741.
(17) Karapanagiotis, I.; Evans, D. F.; Gerberich, W. W. *Langmuir* **2001**, *17*, 3266.
(18) Green, C. P.; Lioe, H.; Cleveland, J. P.; Proksch, R.; Mulvaney, P.; Sader, J. E. *Rev. Sci. Instrum.* **2004**, *75*, 1988 and references therein.
(19) Garcìa, R.; Pérez, R. *Surf. Sci. Rep.* **2002**, *47*, 197.
(20) Wolf, B. *Cryst. Res. Technol.* **2000**, *35*, 377.
(21) Tabor, D. *Hardness of Metals*; Oxford University Press: London, 1951.
(22) Sakai, M. *J. Mater. Res.* **1999**, *14*, 3630.
(23) Flores, A.; Baltà-Calleja, F. J.; Attenburrow, G. E.; Bassett, D. C. *Polymer* **2000**, *41*, 5431.
(24) Johnson, K. L. *Contact mechanics*; Cambridge University Press: Cambridge, U.K., 1985.
(25) Struik, L. C. E. *J. Non-Cryst. Solids* **1991**, *395*, 131.
(26) Flores, A.; Baltà, Calleja, F. J.; Attenburrow, G. E.; Bassett, D. C. *Polymer* **2000**, *41*, 5431.

MA070682B